

Changes in the Electronic Properties of a Molecule When It Is Wired into a Circuit

X. D. Cui,[†] A. Primak,^{‡,§} X. Zarate,[‡] J. Tomfohr,[†] O. F. Sankey,[†] A. L. Moore,[‡] T. A. Moore,[‡] D. Gust,[‡] L. A. Nagahara,[§] and S. M. Lindsay^{*,†}

Department of Physics and Astronomy and Department of Chemistry and Biochemistry, Arizona State University, Tempe, Arizona 85287, and Motorola Inc., 2100 East Elliot Road, AZ34/EL 704, Tempe, Arizona 85284

Received: March 1, 2002; In Final Form: May 27, 2002

Molecular electronic devices require at least two electrical contacts to one (or more) molecule(s). Single molecules are reliably probed by bonding one end to a gold substrate and the other end to a gold nanocrystal. The circuit is completed with a gold-coated atomic force microscope probe. Measurements of the decay of electronic current with the length of *n*-alkanedithiol molecules in these single-molecule nanojunctions are reported as a function of the applied bias. The value of the decay constant near zero bias was obtained from measurements in the ohmic region of the current–voltage curves. The electron tunneling decay rate is significantly smaller ($\beta_N = 0.57 \pm 0.03$) than observed for molecules bonded at just one end ($\beta_N \approx 1$), and it falls to even smaller values as the applied bias is increased. Both these effects are quantitatively accounted for by a large shift in molecular levels caused by the attachment of wires at each end.

Introduction

As a result of the demonstration of operating molecular electronic devices,^{1–4} there is considerable interest in the electronic properties of single molecules wired into electronic circuits. However, the data obtained from measurements on single molecules vary considerably, suggesting that significant experimental difficulties complicate interpretation of the data. This point is starkly illustrated by the controversy over the electronic properties of DNA. This molecule is an electronic insulator,⁵ semiconductor,⁶ metallic conductor,⁷ or superconductor,⁸ depending on which experimental result is chosen. We have studied a much simpler system, the alkanethiols on gold, to clarify some of the difficulties of making electronic measurements on one (or a few) molecule(s).

Much is known about the electronic properties of *n*-alkanethiol monolayers on gold (111) surfaces.^{9–20} Charge is transported by tunneling, current decreasing exponentially with chain length according to $I = I_0 \exp(-\beta_N N)$, where N is the number of methylene groups in the alkane chain, and β_N is found to be about 1 per methylene. β_N shows no dependence on applied bias²⁰ (or electrochemical overpotential¹⁴) over a range of greater than 1 V.

However, there is substantial disagreement between molecular conductivities measured in different experiments, and even greater disagreement with estimates based on quantum transport calculations²⁰ where the disparity can be 5 orders of magnitude or more. Extensive studies of mechanical contacts to alkanethiol monolayers in our laboratory^{20,21} have convinced us that the nonbonded contact in an atomic force microscopic (AFM) or scanning tunneling microscopic (STM) experiment is a source of considerable uncertainty. This is perhaps to be expected, as, outside of an ultrahigh vacuum (UHV) environment, metal surfaces will always be covered with layers of hydrocarbon and water contamination.²²

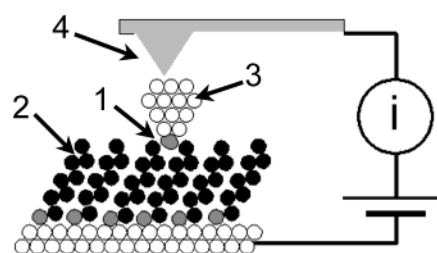


Figure 1. Schematic layout of the single-molecule contact. An alkanedithiol, 1, is inserted into an alkanethiol monolayer on Au(111), 2. The uppermost thiol groups on the dithiols are reacted with gold nanoclusters, 3, from a solution suspension. The tethered clusters are contacted with a gold-coated conducting atomic force microscope probe, 4.

To circumvent problems associated with mechanical, non-bonded contacts, we have developed a covalently bonded single-molecule nanojunction,²³ illustrated schematically in Figure 1. *n*-Alkanedithiols are inserted into a matrix of the corresponding *n*-alkanethiol monolayer on Au(111). The protruding thiol moieties are located by incubating the modified film with a suspension of gold nanocrystals. The assembly is rinsed to remove nonbonded particles, and the film is imaged with a gold-coated atomic force microscope cantilever under an oxygen-free organic solvent. When an attached gold nanoparticle is located, the AFM tip is pushed against it to make a metallic contact to the nanoparticle and thus to the covalently bonded molecule in the gap. The gold nanoparticles as introduced into the toluene solution are coated with and stabilized by ligands, most of which are triphenylphosphine. It is known that these ligands are readily exchanged for alkanethiol ligands upon exposure to the thiol in solution.²⁴ Thus, we postulate that phosphine ligands on the gold nanoparticles in our experiments are displaced by the thiol groups of the alkanedithiols bound to the underlying gold (111) surface in the monolayer. The chemical bonds thus formed prevent washing away of the nanoparticles during rinsing. We further assume that the gold conducting AFM tip is applied to the gold nanoparticles with

[†] Department of Physics and Astronomy, Arizona State University.

[‡] Department of Chemistry and Biochemistry, Arizona State University.

[§] Motorola Inc.

enough force to penetrate the stabilizing coating and make good metal-to-metal electrical contact with the nanoparticle. This is supported by the fact that, once such contact has been made, conduction increases dramatically and then becomes essentially independent of applied force.²³ The precise meaning of “good metal-to-metal” contact on this length scale is an issue discussed later in this paper.

The fact that measured currents are independent of force once a gold contact is made²³ enables accurate and reproducible measurement of the current–voltage (I – V) characteristics of small clusters of connected molecules. The I – V curves fall into clusters that are related to each other as multiples of a fundamental I – V curve, that of a single molecule.²³

In this paper we extend this work to determine the I – V characteristics of a series of n -alkane molecules. We extract the electronic decay constant, β_N , for these molecules as wired into a circuit, and compare it to data obtained for monothiol molecules in self-assembled monolayers.

Theoretical Background

We have discussed a simple barrier-penetration model of a molecule in a metal–molecule–metal gap elsewhere.²⁰ The result of this simple model is that the electronic decay constant, β , depends on the applied bias, V , and the energy difference, ΔE , between the Fermi level and the closest molecular orbital according to

$$\beta(V) = 2\sqrt{\frac{2m^*}{\hbar^2}(\Delta E - \alpha V)} \quad (1)$$

(where β_N is obtained via $\beta_N = 1.25\beta$ in units of \AA^{-1}). In this expression m^* is an effective electron mass, reflecting the strength of the binding potential. In a simple perturbation expansion where the molecular levels are shifted in a uniform electric field, $\alpha = 1/2$ and the shift is the same in both directions of bias. In general, the field distribution across the molecule may be quite complex,²⁵ and we discuss the consequences of this uncertainty later in this paper.

We carry out first principles calculations of the current following Mujica et al.^{26,27}

$$I = \frac{2\pi e}{\hbar} \sum_{if} |T_{fi}|^2 (f(E_i) - f(E_f)) \delta(E_i - E_f + eV) \quad (2)$$

Here, f is the Fermi function and the T matrix elements are calculated from the Green’s function for the coupled metal–molecule–metal system as described elsewhere.²⁰ The voltage dependence of the current was incorporated solely by shifting the energy levels of the high and low voltage contacts by $-eV/2$ and $+eV/2$, respectively. The energies in eq 2 are the zero voltage energies. In some versions of this formula the energies are defined so as to incorporate the applied bias, in which case the term eV does not appear in the delta function. Electronic structure is calculated using Fireball-96 and SIESTA, density functional theory based methods within the pseudopotential approximation.^{28–31} Fireball uses a nonorthogonal basis set of slightly excited²⁹ pseudoatomic orbitals, including an s -state for H, sp_3 for C and S, and sp_3d_5 for Au, allowing geometry optimization to be performed with Hellmann–Feynman forces. The terminal hydrogen atoms on the sulfurs were removed (leaving a neutral thio radical) and the structure relaxed as described under Theoretical Results. These calculations yielded the electronic spectrum for the complete metal–molecule–metal system. From this, the location of the Fermi level relative to

the molecular orbital energies can be determined. Beta (β) was obtained from the currents calculated for different alkane chain lengths. Many of these calculations were repeated with extended basis sets and with plane wave basis sets, and very little dependence on the basis sets was found.³²

The data reported here suggest that there is, in practice, considerable uncertainty about the location of the Fermi level, so we used a method of calculating β as a function of this energy difference based on complex band structure calculations for long chains.³²

Experimental Section

Alkanethiol monolayers were formed from 1 mM solutions in toluene left in contact with flame-annealed Au(111)³³ overnight. Mixed monolayers were formed by overnight incubation of octanethiol, decanethiol, and dodecanethiol monolayers on Au(111) in a 1 mM solution of the corresponding dithiol in toluene.³⁴ Alkanethiols and dithiols were obtained from Aldrich and used without further purification. Freshly prepared gold nanoparticles of core diameter less than 2 nm²⁴ were suspended to a concentration of 0.25 g/L in dichloromethane and incubated with the mixed monolayers overnight. The resulting films were rinsed in dichloromethane and then toluene, and were subsequently imaged in toluene. Isolated conducting particles of gold attached to the monolayer were observed and used as contact points for a freshly prepared gold-coated AFM probe.

Measurements were made using a PicoSPM conducting atomic force microscope (Molecular Imaging, Phoenix) using a hermetically sealed sample chamber flushed with nitrogen to reduce oxygen and water vapor contamination. Silicon cantilevers with a spring constant of 0.35 N/m (Molecular Imaging) were sputter-coated with 5 nm of Cr followed by 50 nm of Au. Contamination was reduced further by submerging the sample in freshly distilled toluene. This also eliminates adhesion between the AFM tip and the sample, permitting controlled contact between the tip and gold nanocrystals.

Current vs voltage (I – V) data were obtained by repeated cycling from small bias ranges with the range increased incrementally to determine the highest bias that could be applied without altering the electrical properties of the molecules. This critical bias was found to be substantially less than could be applied using a mechanical contact. In the case of octanedithiol, curves were altered when the bias exceeded ± 1 V, compared to the ± 3 V that could be applied to an octanethiol monolayer (with the same level of environmental control).²⁰

Results and Discussion

Conducting AFM Results. As reported previously for octanedithiols,²³ distinct families of I – V curves were observed as shown in Figures 2a (octanedithiols), 3a (decanedithiols), and 4a (dodecanedithiols). Each family is an integer multiple of a fundamental I – V curve, that of a single molecule.²³ This is demonstrated by finding the value of a divisor that minimizes the variance between any pair of curves. When this divisor was determined for a large number of curves and presented as a histogram, peaks are found at integer values, 1, 2, 3, 4 (and on up to 7 in some cases). These histograms are shown for each molecule in Figures 2b, 3b, and 4b. In this way, the curves associated with clusters of one, two, three, and four molecules are identified.

A current-decay constant, β_N , was calculated at each voltage for each family of curves by fitting the current to $I(V) = I_0(V) \exp[-\beta_N(V)N]$ for $N = 8, 10, \text{ and } 12$. The means and standard deviations of these values for each family of molecular clusters

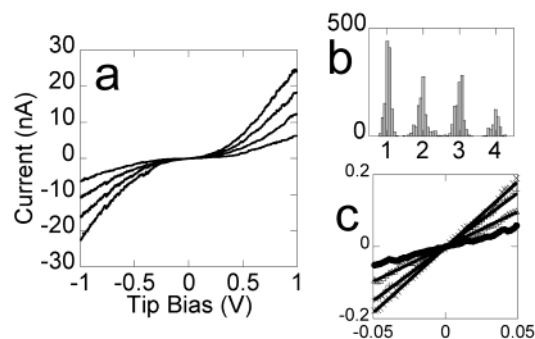


Figure 2. (a) Current–voltage (I – V) data for clusters of octanedithiol molecules inserted into octanemonothiol monolayers. (b) Histogram plot of the value of a divisor that minimizes variance between any pair of I – V curves. (c) I – V data in the ohmic region (-50 mV $< V < +50$ mV). Solid lines are linear fits yielding resistances of 965 ± 20 M Ω (one molecule cluster, $n = 56$), 517 ± 10 M Ω (two molecule clusters, $n = 25$), 333 ± 8 M Ω (three molecule clusters, $n = 20$), and 274 ± 5 M Ω (four molecule clusters, $n = 15$).

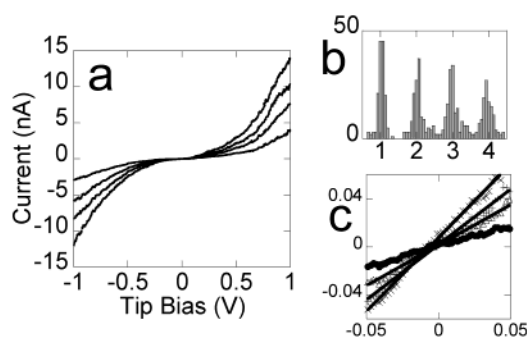


Figure 3. (a) Current–voltage (I – V) data for clusters of decanedithiol molecules inserted into decanemonothiol monolayers. (b) Histogram plot of the value of a divisor that minimizes variance between any pair of I – V curves. (c) I – V data in the ohmic region (-50 mV $< V < +50$ mV). Solid lines are linear fits yielding resistances of 2.89 ± 0.5 G Ω (one molecule cluster, $n = 42$), 1.48 ± 0.3 G Ω (two molecule clusters, $n = 20$), 1.08 ± 0.2 G Ω (three molecule clusters, $n = 15$), and 819 ± 100 M Ω (four molecule clusters, $n = 10$).

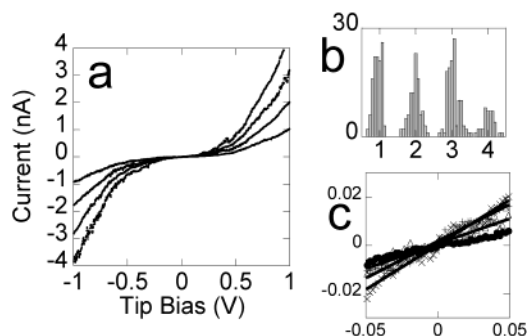


Figure 4. (a) Current–voltage (I – V) data for clusters of dodecanedithiol molecules inserted into dodecanemonothiol monolayers. (b) Histogram plot of the value of a divisor that minimizes variance between any pair of I – V curves. (c) I – V data in the ohmic region (-50 mV $< V < +50$ mV). Solid lines are linear fits yielding resistances of 8.26 ± 1 G Ω (one molecule cluster, $n = 27$), 4.8 ± 0.6 G Ω (two molecule clusters, $n = 14$), 3.27 ± 0.6 G Ω (three molecule clusters, $n = 11$), and 2.68 ± 0.5 G Ω (four molecule clusters, $n = 8$).

(one, two, three, and four molecules) at each voltage are shown in Figure 5. These values of β_N are significantly smaller than those obtained from molecules chemically bonded to a metal at just one end where $\beta_N \approx 1$.^{15–20} Further, β_N decreases markedly as the applied bias is increased (Figure 5), an effect that is not observed in alkanethiol monolayers bonded to just one electrode.^{14,20} Note that the standard deviations on the data

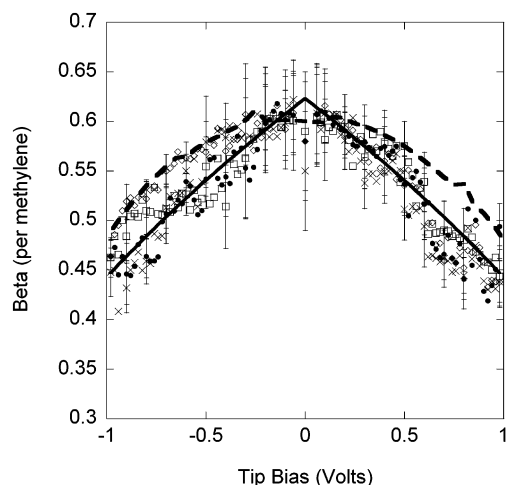


Figure 5. Electronic decay constant, β_N , in units of (methylene)^{–1} for clusters of one molecule (●), two molecules (□), three molecules (◇), and four molecules (×). The data at zero bias were derived from log plots of the resistances as described in Figure 6. Representative error bars are ± 1 SD. The solid line is the rectangular barrier theory (eq 1) with $m^* = 0.16m_e$ and $\Delta E = 1.3$ eV. The dashed curve is the first principles calculation carried out as explained in the text.

points are very much smaller than those obtained from measurements with mechanical contacts.²⁰ Each data point is obtained from around 100 curves, so the standard errors are substantially smaller than the standard deviations shown in the figure. Thus, the observed voltage dependence cannot be ascribed to experimental uncertainties.

This small value of β_N and its voltage dependence are quite unexpected results. It is clear that the bonded contacts have changed the field distribution across the molecules because the lower breakdown voltage of the bonded molecules suggests that more of the applied field appears across the molecule (as opposed to the gap between a contact and a molecule). If this is the case, then perhaps significant changes could occur even at very small biases. For this reason, we explored the linear, ohmic region of the I – V curves at low bias carefully in order to determine $\beta_N(0)$. Data collection at low bias is complicated by leakage current caused by residual ionic contamination of the toluene used to control adhesion and contamination. For this reason, curves were selected from runs in which leakage current was immeasurably small. Ohmic behavior is found for biases between ± 50 mV as shown in Figures 2c, 3c, and 3d. The corresponding resistances are listed in the figure captions. Within experimental uncertainties, these resistances are in the ratios 1:0.5:0.33:0.25, showing that the currents through the molecular clusters add as would be expected for parallel combinations of one, two, three, and four equal resistors. It is not obvious that this should be the case, because quantum interference and interactions between neighboring molecules could result in a more complex addition of currents.

These resistance data are used to derive values for β_N at zero bias as shown in Figure 6. The corresponding values of β_N are listed in the figure caption. They are all equal to 0.57 within experimental error. Thus, these low voltage measurements show that β_N is indeed intrinsically small for these molecules bonded into metallic contacts.

The value of β_N at low bias is also important because electron tunneling theory relates $\beta_N(V)$ to the value of β_N at zero bias. As can be seen from eq 1, a small $\beta_N(0)$ implies a significant voltage dependence. Our data (Figure 5) show that β_N depends

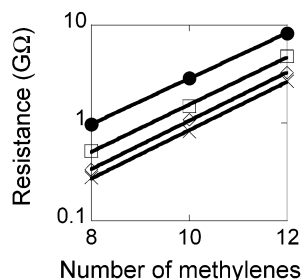


Figure 6. Resistances of one- (●), two- (□), three- (◇), and four- (×) molecule clusters as a function of alkane chain length plotted as log resistance vs number of methylene groups. The straight lines are exponential fits yielding β at zero bias as 0.58 ± 0.06 (one molecule cluster), 0.59 ± 0.06 (two molecule clusters), 0.58 ± 0.06 (three molecule clusters), and 0.55 ± 0.06 (four molecule clusters).

on bias, so we now turn to an examination of the relationship between $\beta_N(0)$ and $\beta_N(V)$ in terms of theories of electron tunneling.

Theoretical Calculations. The solid line in Figure 5 shows a fit of our data with eq 1 using $m^* = 0.16m_e$ and $\Delta E = 1.3$ eV with $\alpha = 0.5$. Clearly, the unexpectedly low value of β_N and its voltage dependence are accounted for by this value of ΔE . ΔE can be estimated from the ionization potentials of alkanes³⁵ and the work function of gold, yielding a value of approximately 5 eV. The unexpectedly low value for β_N and its voltage dependence translate into an unexpectedly low value for ΔE . A first principles calculation leads to a similar conclusion, at variance with our experimentally determined value.

Using electronic structure methods removes the need for both of the fitting parameters, ΔE and m^* .²³ The metal–molecule–metal system was modeled the following way (for details see Tomfohr and Sankey³²): Green’s function was determined for an infinite array of the molecules in a $\sqrt{3} \times \sqrt{3}$ array tethered between gold sheets of eight atoms thickness (with the structure relaxed as described elsewhere³²). The unit cell of the supercell contains six layers of 111 gold with one alkane per $\sqrt{3} \times \sqrt{3}$ gold surface atom. Thicker layers of Au (up to 12 atoms) were explored, and similar results were found. This supercell incorporates intermolecular interactions and the electronic structure of the gold surface as bonded to the molecules. A preferred orientation of the molecule was determined by structural relaxation. The Au atoms were fixed and the end thio radical was initially located above the 3-fold hollow site of the Au(111) surface. The bond lengths and bond angles of the chain were fixed at their ideal values. The resulting Au–S bond lengths are 2.56 Å. The tilt of the molecule is about 30° from the surface normal. Further details can be found in ref 32. The Dyson equation was then used to couple the gold slabs midway (i.e., four atoms depth) to semi-infinite slabs of gold. In this way, the contribution of both surface states and the bulk density of states to current could be calculated, dealing with the charge distribution for the system self-consistently.

The electronic density of states for gold–octanedithiol–gold is shown as the solid line in Figure 7. The Fermi level is set to 0 V, so it can be seen that the gap to either the HOMO or LUMO is indeed about 5 eV. The magnitude of currents calculated with eq 2 are in reasonable agreement with the observed currents for a single molecule²³ but the shape of the I – V curve is not: the experimentally measured curve turns on more sharply than the calculated curve. β_N can be calculated directly from the currents calculated using eq 2 for the series octanedithiol, decanedithiol, and dodecanedithiol, and the result

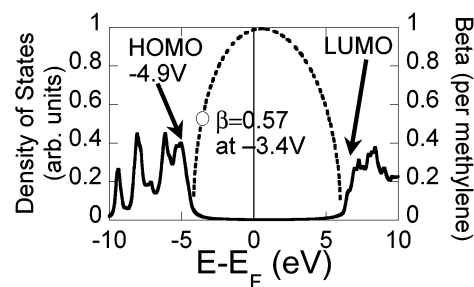


Figure 7. Calculated density of states (DOS, solid line, left axis) for an octanedithiol SAM between gold electrodes. The plot is of the DOS projected onto the orbitals of one of the carbons in the middle of the octane molecule (fourth from the end). This reveals the locations of the HOMO and LUMO relative to the Fermi level (at 0 eV). Complex band structure calculations (dashed line) yield β (per methylene) for any value of the gap between the Fermi level and the molecular orbitals. In this case, the smallest β is obtained for interaction with the HOMO (as $E - E_F$ approaches -5 V) or the LUMO (as $E - E_F$ approaches $+5$ V). The first principles calculation places the Fermi level in the middle of the HOMO–LUMO gap as shown in the figure. This implies that β is about 1 per methylene. Agreement with the experimentally determined value of β requires shifting the Fermi level down by 3.4 eV.

is that β is about 1 per methylene and does not depend on bias, in complete disagreement with the measured data.

In view of the discrepancy between the value of ΔE obtained by fitting eq 1 (1.3 eV) and the values obtained from the simulation (ca. 5 eV), we sought to investigate the dependence of β on ΔE using complex band structure calculations.³² The result is plotted as the dashed curve in Figure 7. Fitting the measured $\beta_N(0)$ requires shifting the Fermi level by 3.4 eV so that $\Delta E = 1.5$ eV (close to what was obtained with the simple model). Fixing the Fermi level at this value and recalculating the currents using eq 2 yields the voltage dependence, $\beta_N(V)$, as well as its absolute value, and the results are shown as the dashed line in Figure 5. Thus, adjusting ΔE to an unexpectedly low value yields the same result as the simple theory: both the low value of $\beta_N(0)$ and the voltage dependence, $\beta_N(V)$, are quantitatively accounted for. The simulation achieves this with one less parameter than the simple model (the effective electron mass). This quantity can be calculated directly from the band structure, yielding $m^* = 0.2m_e$ close to the value obtained by fitting the data to eq 1.

The meaning of an effective mass in this context is discussed in detail elsewhere.³² Briefly, the tunneling states come from bonding and antibonding σ -bonded states along the chain. The states for a finite chain are a subset of the states for an infinite chain, much like the harmonics of a finite length string are a subset of the harmonics of those of a very long string. For allowed points for the finite chain that are near the band edge for the infinite chain, β has the form of eq 1 with the effective mass given by that of the parent (infinite chain) band by $1/m^* = (1/\hbar^2)(\partial^2 E/\partial k^2)$.

The simulation used an electric field that had half the voltage drop at the left interface and half the voltage drop at the right interface (corresponding to $\alpha = 1/2$ in eq 1), and the actual potential distribution may be quite different.²⁵ However, this simplification cannot account for the calculated small value of ΔE , because the voltage distribution does not enter into the calculation of $\beta_N(0)$ (though it might affect the experiment—see below). Furthermore, the symmetry of the measured I – V curves requires that $\alpha = 1/2$. Values other than 1/2 correspond to more rapid approach to resonance in one direction of bias, whatever the details of potential distribution in the gap. The same result holds in the electronic structure calculation where

a symmetrical potential distribution is found to have no effect to first order in perturbation theory. These results proved relatively insensitive to the precise details of the metal–molecule coupling geometry or the basis set used in the calculation (extended local orbital or plane wave). Better fits were obtained when the Fermi level was moved toward the HOMO (as shown in Figure 3), but we cannot rule out LUMO-mediated tunneling.

One consequence of shifting the Fermi level in this way is a large increase in calculated currents (several hundred fold) as resonance is now more closely approached. It should be noted that the single-molecule currents that we measure, and the current calculated by extrapolating electrochemical rate constant data to zero thermal activation (appropriate for metal “donors” and “acceptors” of electrons) are in close agreement (S. E. Creager, personal communication). Therefore, it appears eq 2 does not adequately describe charge transport in these molecules.

We are left with the surprising conclusion that the energy difference between the Fermi level and the molecular orbital(s) that mediate tunneling is very different in a molecule contacted at both ends compared to a molecule tethered to a gold surface at one end only.²⁰ In the case of a mechanical contact to the top of a monolayer, the current changes with compression of the film in a manner accounted for by chain-to-chain tunneling.^{11,20} The current through molecules bonded at each end does not change as the film is compressed, a result accounted for by through-bond tunneling^{11,23} (this also rules out a mechanical explanation for the difference between one- and two-bonded contacts). Perhaps this change in effective tunneling path is responsible for the differences in $\beta_N(0)$ and $\beta_N(V)$, though current theoretical models give no hint of a mechanism.

Large changes in the properties of molecules connected to electrodes have been determined by other methods. Martel et al.³⁶ have determined the gap between the Fermi level and states of a single-walled semiconducting carbon nanotube from the temperature dependence of carrier injection, finding $\Delta E = 15$ meV, 20 times smaller than the expected value of 300 meV, an effect they attribute to unknown properties of the molecule–metal contacts. Photoelectron spectroscopies have been used to determine large shifts in the energies of molecular orbitals on binding to metal surfaces,^{37–39} an effect at least partially accounted for by the dipole associated with the formation of the molecule–metal bond.⁴⁰

The studies discussed above do not address the large difference between the value of $\beta_N(0)$ as determined for alkanethiols covalently connected to a metal at one end only²⁰ and the value of $\beta_N(0)$ as determined for alkanedithiols connected between two metal contacts. As discussed above, the stress dependence of tunnel current suggests that the mechanism of charge transfer is altered in a fundamental manner. There is, in addition, a subtle, but possibly important effect that has not been considered previously. This is the distortion of measurements of β caused by the dependence of the potential distribution on the length of the molecule in the gap. It is clear that such an effect can exist for the case of a “poor” (i.e., mechanical) contact at one end of the molecule because the potential drop across the molecule will reflect the ratio of the top “contact resistance” to the molecular resistance, and this quantity will change with the length of the molecule. This will, in turn, distort the value of β obtained from comparing the currents obtained with different lengths of molecule at a given overall bias.

At first glance, our method of making “good” contacts circumvents this distortion of the data. However, these contacts are not classical. Even if a “good” metallic bond is made between the coated AFM tip and the gold nanoparticle, it is

unlikely to extend over many atomic diameters and is therefore unlikely to be very much bigger than the Fermi wavelength of the electrons, so that the contact resistance is unlikely to be much less than the resistance quantum (12.6 k Ω).^{27,41} Small though such a resistance sounds in this context, it is large enough to enable the gold nanoparticle to charge separately from the bulk electrode, forming a Coulomb blockade.⁴² This will set up two different potential distributions, above and below the blockade threshold, changing the role of the gold nanoparticle in the charge transport in a potential-dependent way. It is hoped that a detailed analysis of current–voltage data will shed light on this.

Conclusions

The electronic decay constant per methylene at zero bias, $\beta_N(0)$, is determined to be 0.57 ± 0.03 (standard error) in clusters of one, two, three, and four octanedithiol, decanedithiol, and dodecanedithiol molecules covalently tethered between gold contacts. It falls to about 0.47 when a bias of ± 1 V is applied to the metal–molecule–metal assembly. These values are significantly smaller than those determined by measurements on alkanethiol monolayers, and also significantly smaller than predictions based on self-consistent first principles electronic structure calculations. The small value of $\beta_N(0)$ and its voltage dependence, $\beta_N(V)$, are quantitatively accounted for by a 3-fold reduction in the gap between the Fermi level and a molecular orbital from ca. 5 to 1.5 eV. The origin of this reduction remains obscure, but similar effects have been observed in other molecules. The difference between $\beta_N(0)$ as measured for alkanethiol monolayers and as measured for alkanedithiol molecules between gold contacts remains unaccounted for, though it is clear that the tunneling mechanism is changed. Modification of the potential distribution by Coulomb blockading may also play a role.

Acknowledgment. This work was supported by the NSF (ECS 01101175 and CHE 0078835) and Molecular Imaging. We thank Marshall Newton and Mark Ratner for comments on the manuscript.

References and Notes

- (1) Reed, M. A.; Zhou, C.; Muller, C. J.; Burgin, T. P.; Tour, J. M. *Science* **1997**, *278*, 252–254.
- (2) Chen, J.; Reed, M. A.; Rawlett, M. A.; Tour, J. M. *Science* **1999**, *286*, 1550–1552.
- (3) Collier, C. J.; Wong, E. W.; Belohradsky, M.; Raymo, F. M.; Stoddart, J. F.; Kuekes, P. J.; Williams, R. S.; Heath, J. R. *Science* **1999**, *285*, 391–394.
- (4) Schon, J. H.; Meng, H.; Bao, Z. *Nature* **2001**, *413*, 713–716.
- (5) Dunlap, D. D.; Garcia, R.; Schabtach, E.; Bustamante, C. *Proc. Natl. Acad. Sci. U.S.A.* **1993**, *90*, 7652–7655.
- (6) Porath, D.; Bezryadin, A.; de Vries, S.; Dekkar, C. *Nature* **2000**, *403*, 635–638.
- (7) Fink, H.-W.; Schoenberger, C. *Nature* **1999**, *398*, 407–410.
- (8) Kasumov, A. Y.; Kociak, M.; Guéron, S.; Reulet, B.; Volkov, V. T.; Klinov, D. V.; Bouchiat, H. *Science* **2001**, *291*, 280–282.
- (9) Duwez, A. S.; Di Paolo, S.; Ghijsen, J.; Riga, J.; DeLeuze, M.; Delhalle, J. *J. Phys. Chem. B* **1997**, *101*, 884–890.
- (10) Miller, C.; Cuendet, P.; Gratzel, M. *J. Phys. Chem.* **1991**, *95*, 877–886.
- (11) Slowinski, K.; Chamberlain, R. V.; Miller, C. J.; Majda, M. *J. Am. Chem. Soc.* **1997**, *119*, 11910–11919.
- (12) Chidsey, C. E. D. *Science* **1991**, *251*, 919–922.
- (13) Smalley, J. N.; Feldberg, S. W.; Chidsey, C. E. D.; Linford, M. R.; Newton, M. D.; Liu, Y. P. *J. Phys. Chem.* **1995**, *99*, 13141–13149.
- (14) Becka, A. M.; Miller, C. J. *J. Phys. Chem.* **1992**, *96*, 2657–2668.
- (15) Slowinski, K.; Fong, H. K. Y.; Majda, M. *J. Am. Chem. Soc.* **1999**, *121*, 7257–7261.

- (16) Holmlin, E.; Haag, R.; Chabinye, M. L.; Ismagilov, R. F.; Cohen, A. E.; Terfort, A.; Rampi, M. A.; Whitesides, G. M. *J. Am. Chem. Soc.* **2001**, *123*, 5075–5085.
- (17) Bumm, L. A.; Arnold, J. J.; Dunbar, T. D.; Allara, D. L.; Weiss, P. S. *J. Phys. Chem.* **1999**, *103*, 8122–8127.
- (18) Salmeron, M.; Neubauer, G.; Folch, A.; Tomitori, M.; Ogletree, D. F.; Sautet, P. *Langmuir* **1993**, *9*, 3600–3611.
- (19) Wold, D. J.; Frisbie, C. D. *J. Am. Chem. Soc.* **2000**, *122*, 2970–2971.
- (20) Cui, X. D.; Zarate, X.; Tomfohr, J.; Primak, A.; Moore, A. L.; Moore, T. A.; Gust, D.; Harris, G.; Sankey, O. F.; Lindsay, S. M. *Nanotechnology* **2002**, *13*, 5–14.
- (21) Cui, X. D.; Zarate, X.; Tomfohr, J.; Primak, A.; Moore, A. L.; Moore, T. A.; Gust, D.; Harris, G.; Sankey, O. F.; Lindsay, S. M. *Ultramicroscopy* **2002**, *92*, 67–96.
- (22) Smith, T. J. *Colloid Interface Sci.* **1980**, *75*, 51–53.
- (23) Cui, X. D.; Primak, A.; Zarate, X.; Tomfohr, J.; Sankey, O. F.; Moore, A. L.; Moore, T. A.; Gust, D.; G., H.; Lindsay, S. M. *Science* **2001**, *294*, 571–574.
- (24) Weare, W. W.; Reed, S. M.; Warner, M. G.; Huchison, J. E. *J. Am. Chem. Soc.* **2000**, *122*, 12890–12891.
- (25) Mujica, V.; Roitberg, A. E.; Ratner, M. *J. Chem. Phys.* **2000**, *112*, 6834–6839.
- (26) Mujica, V.; Kemp, M.; Ratner, M. A. *J. Chem. Phys.* **1994**, *101*, 6849–6855.
- (27) Datta, S. *Electronic transport in mesoscopic systems*; Cambridge University Press: Cambridge, UK, 1990.
- (28) Demkov, A. A.; Ortega, J.; Sankey, O. F.; Grumbach, M. P. *Phys. Rev. B* **1995**, *52*, 1618.
- (29) Sankey, O. F.; Demkov, A. A.; Windl, W.; Fritsch, J. H.; Lewis, J. P.; Fuentes-Cabrera, M. *Int. J. Quantum Chem.* **1998**, *69*, 327.
- (30) Ordejon, P.; Artacho, E.; Soler, J. M. *Phys. Rev. B* **1996**, *53*, 10441–10444.
- (31) Sanchez-Portal, D.; Ordejon, P.; Artacho, E.; Soler, J. M. *Int. J. Quantum Chem.* **1997**, *65*, 453–461.
- (32) Tomfohr, J.; Sankey, O. F. *Phys. Rev. B* **2002**, *65*, 245105.
- (33) DeRose, J. A.; Thundat, T.; Nagahara, L. A.; Lindsay, S. M. *Surf. Sci.* **1991**, *256*, 102–108.
- (34) Cygan, M. T.; Dunbar, T. D.; Arnold, J. J.; Bumm, L. A.; Shedlock, N. F.; Burgin, T. P.; Jones, L.; Allara, D. L.; Tour, J. M.; Weiss, P. S. *J. Am. Chem. Soc.* **1998**, *120*, 2721–2732.
- (35) Henry, H.; Fliszar, S. *Can. J. Chem.* **1974**, *52*, 3799–3802.
- (36) Martel, R.; Derycke, V.; Lavoie, C.; Appenzeller, J.; K. K., C.; Tersoff, J.; Avouris, P. *Phys. Rev. Lett.* **2001**, *87*, 1–4.
- (37) Vondrak, T.; Cramer, T.; Zhu, X.-Y. *J. Phys. Chem. B* **1999**, *103*, 8915–8919.
- (38) Wang, H.; Dutton, G.; Zhu, X.-Y. *J. Phys. Chem. B* **2000**, *104*, 10332–10338.
- (39) Hill, I. G.; Mäkinen, A. J.; Kafafi, Z. H. *J. Appl. Phys.* **2000**, *88*, 889–895.
- (40) Xue, Y.; Datta, S.; Ratner, M. *J. Chem. Phys.* **2001**, *115*, 4292–4299.
- (41) Imry, Y. *Physics of Mesoscopic Systems*. In *Directions in Condensed Matter Physics*; Grinstein, G., Mazenko, G., Eds.; World Scientific Publishing: Philadelphia, 1986; Vol. 1, pp 101–163.
- (42) Hanna, A. E.; Tinkham, M. *Phys. Rev. B* **1991**, *44*, 5919–5922.